Participation in the Analysis of the Far-Infrared/Submillimeter Interferometer

Annual Report #1

NASA Grant NNG04GQ21G

For the period 1 September 2004 through 30 June 2005

Principal Investigator

Enrico C. Lorenzini

July 2005

Prepared for
National Aeronautics and Space Administration
Goddard Space Flight Center, Maryland, 20771

Smithsonian Institution
Astrophysical Observatory
Cambridge, Massachusetts 02138

The Smithsonian Astrophysical Observatory
is a member of the
Harvard-Smithsonian Center for Astrophysics

Participation in the Analysis of the Far-Infrared/Submillimeter Interferometer

Annual Report #1

NASA Grant NNG04GQ21G

For the period 1 September 2004 through 30 June 2005

Principal Investigator

Enrico C. Lorenzini

Co-Investigator

Claudio Bombardelli

July 2005

Prepared for
National Aeronautics and Space Administration
Goddard Space Flight Center, Maryland, 20771

Smithsonian Institution
Astrophysical Observatory
Cambridge, Massachusetts 02138

The Smithsonian Astrophysical Observatory
is a member of the
Harvard-Smithsonian Center for Astrophysics

TABLE OF CONTENTS

Abstract

We have contributed to the development of the Submillimiter Probe of the Evolution of Cosmic Structure (SPECS) by analyzing various aspects related to the tethers that connect the spacecraft of this space interferometer. We have focused our analysis on key topics as follows: (a) helping in the configuration selection; (b) computing the system eigenfrequencies as a function of baseline length; (c) developing techniques and conceptual design of devices for damping the tether oscillations; (d) carrying out numerical simulations of tethered formation to assess the effects of environmental perturbations upon the baseline length variation; (e) devising control laws for fast retargeting of the interferometer at moderate baseline lengths; (f) estimating the survivability to micrometeoroid impacts of a tether at L2; and (g) developing a conceptual design of a high-strength and survivable tether.

Introduction

The Submillimiter Probe for the Evolution of Cosmic Structure[i] (SPECS) is a spaced-based interferometer consisting of a set of spacecraft flying in formation at the Sun-Earth Lagrange point L-2. SPECS is an imaging interferometer operating at a baseline length ranging from about 20 m to 1 km. The telescopes (collector spacecraft) will be spiraling inward or outward to fill (without a need for 100% coverage) the annular space bounded by the minimum and maximum baseline lengths to make an image. The light collected at the collectors is beamed to a central combiner where the light beams are compared to form the interference fringes. SPECS operates in the far-infrared/submillimiter wavelengths with a range between 50 μm and 400 μm. This implies a maximum angular resolution (at the longest baseline length) of 50 milliarcsec, which is comparable to the resolution of the Hubble Space Telescope in the optical wave band.

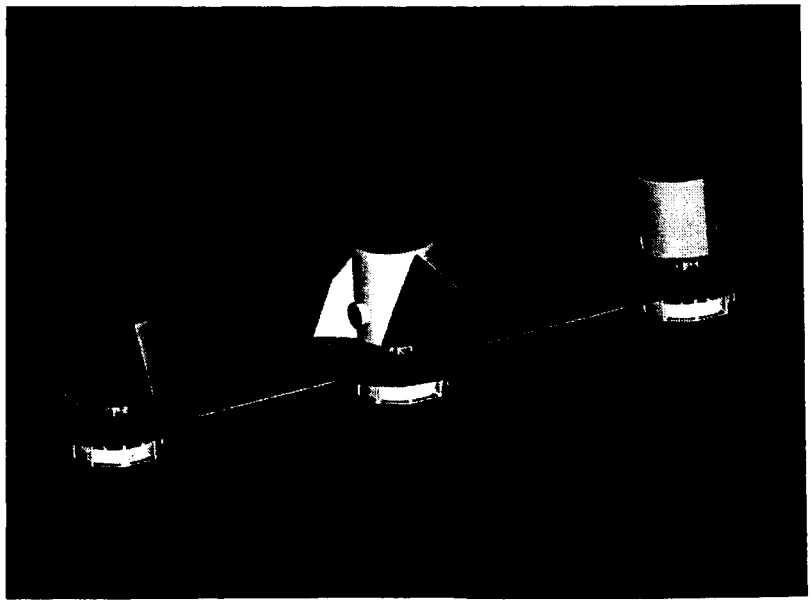

Figure 1 Artist's rendition of the present configuration of SPECS.

In its present configuration (see Fig. 1), SPECS consists of two 4-m-diameter telescopes (on the collector spacecraft) and one central combiner spacecraft, all arranged in an in-line configuration where the combiner is at the hub. As mentioned previously, an image of the target source is formed by slowly spinning the linear configuration about the hub (combiner) while the

baseline length (between the two collectors) is increased or alternatively decreased to span the entire u-v plane.

The science goals call for a minimum 5-year mission with 1500 targets observed. The requirement of an average of one target per day implies spinning the formation with a period of typically 25 minutes. The propellant required to keep the formation together over the 5-year time would be absolutely prohibitive with free flyers even if using the most efficient electrical thrusters. Tethers are an obvious choice to provide the centripetal accelerations that keep the formation together without consuming propellant except for changes of angular momentum (both in term of direction and magnitude).

This report presents the results of the analysis carried out during the last-year grant activity on the dynamics, control, and preliminary design of the tether system for SPECS.

Considerations on Tethered Interferometer Configurations

The engineering analysis conducted at NASA Goddard indicated that the SPECS spacecraft will be massive. Consequently, the primary limit in launching all the spacecraft together will originate from the payload capacity of the launcher and, in turn, we need to limit the number of spacecraft to the minimum required for interferometry. In other words, we need to focus our attention on tethered configurations that consist of two collectors and one combiner.

In the following we list a number of pros and cons of different configurations for a tethered interferometer made of three spacecraft. This is far from a comprehensive analysis of the various configurations but is meant to provide some guidelines for the configuration selection.

Linear Configuration

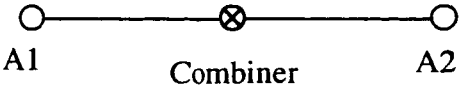

Figure 2 Schematic of linear configuration with two collectors.

Pros:

- Fewer parts and mechanisms for tether control;
- Deployment of formation in space is easier and similar to deployment of previous tethered mission in LEO;
- No wobbling orthogonally to the spin plane in the absence of perturbing torques;
- Easiness of retargeting: the linear configuration simply needs to rotate the spin plane without requiring control of the out-of-plane motion as for a 2-D configuration;
- Distance collector-combiner is minimized.

Cons:

- Collector tangential velocity is coupled to baseline length ('ballerina effect'): the speed increase with decreasing baseline length requires momentum management control;
- Collectors and combiner can rotate about tether line and require attitude control;
- Single-line metrology can lead to lower accuracy position determination.

Variable-Triangle Configuration

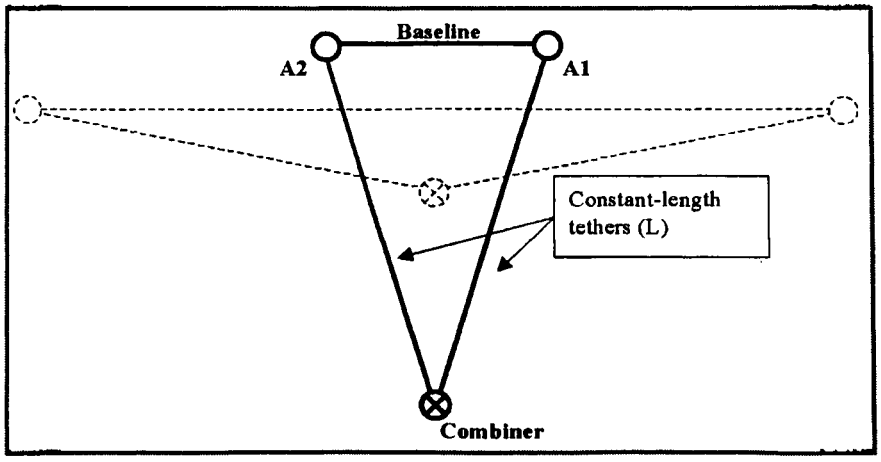

Figure 3 Schematic of a single baseline variable-triangle configuration

Pros:

- Only one tether reel at the baseline needed for u-v scan;

- Constant distance from collectors to combiner during u-v coverage: reeling of baseline does not affect OPD to first order;
- Combiner acts as a 'ballast': tangential speed of collector is almost decoupled from baseline variation. A fairly constant speed can be obtained in combination with constant angular momentum;
- More accurate position determination thanks to multi-line metrology;
- Two-point support of collectors and combiner, i.e., better attitude control of spacecraft.

Cons:

- Retargeting requires added control/thrusting to keep the formation planar;
- Initial deployment of formation is more complex;
- Mirrors on combiner must track the collectors during baseline changes which is difficult to do with a cryogenic design;
- More parts and reel mechanisms than for linear configuration;
- The distances collector-combiner are higher than in linear configuration leading to losses of transmitted signal.

Equilateral-Triangle Configuration

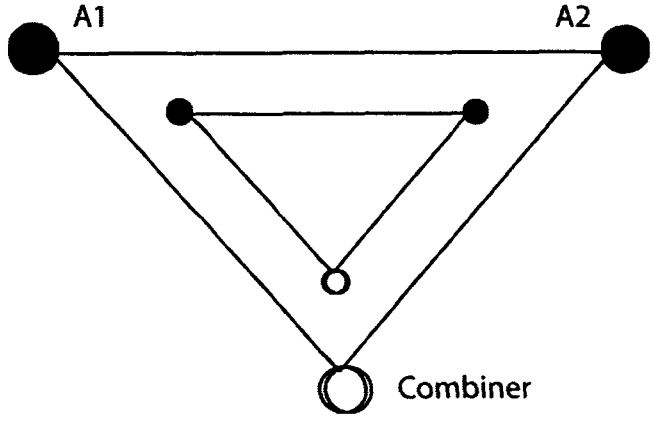

Figure 4 Schematic of a single baseline equilateral-triangle configuration

Pros:

- More accurate position determination thanks to multi-line metrology;

- Constant viewing angles from combiner to collectors (however the angles need to be maintained accurately);
- Two-point support of collectors and combiner, i.e., better attitude control.

Cons:

- Retargeting requires added control/thrusting to keep the formation planar;
- Initial deployment of formation is comparatively complex;
- More parts and reel mechanisms than for linear configuration;
- The distances collector-combiner are higher than in linear configuration leading to losses of transmitted signal.

In conclusion, the linear configuration was selected by the SPECS team as the best compromise between simplicity and performance.

Tether and Tether-related Oscillation Frequencies

Constant spin rate of the interferometer

The oscillation modes of the linear formation are grouped into:

a) tether longitudinal waves;
b) tether transverse waves;
c) motions of spacecraft attached to the elastic tethers.

We have assumed: collector mass = 3200 kg, combiner mass = 3500 kg, tether linear density = 0.03 kg/m, and longitudinal tether stiffness EA = 10^6 N. The spin rate of the interferometer was assumed equal to 0.004 rad/s at all baseline lengths. Note that the spin rate only affects the transverse waves' frequencies and the butterfly mode frequency, which are both directly proportional to it.

Longitudinal tether waves are naturally damped by the internal friction of the tether more quickly than all the other modes. Transverse tether waves will be damped by the tether attachment point dampers over a time of typically a few minutes for the lowest frequency waves and shorter for the higher-frequency waves. Bobbing frequencies (i.e., the stretching of the elastic tethers due to the massive satellites attached to them) can be damped by the tether reels.

The plot in Figure 5 shows the frequencies of tether waves and spacecraft motions associated with the tether constraints vs. the baseline length.

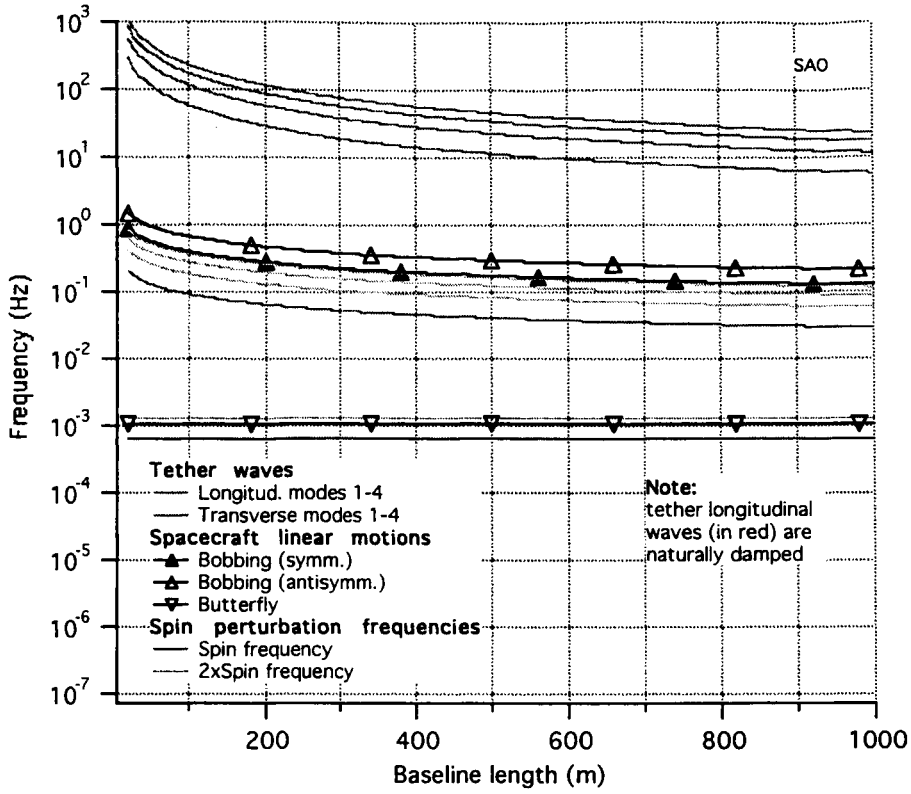

Figure 5 Frequencies vs. baseline length for constant spin rate of the interferometer.

The butterfly mode consists of the collectors moving sideways with respect to the combiner (like flapping wings). The butterfly frequency is independent of tether stiffness. For small oscillations this mode is decoupled from tether stretches and, most likely, will require propulsion forces for damping it out, once excited. Among other causes, the butterfly mode can be excited by differential solar radiation forces produced by unequal ballistic coefficients between collectors and combiner. The amplitude of the butterfly mode grows with time if the butterfly frequency is equal to twice the spin frequency (i.e., a resonant condition). Fortunately, the growth rate is very slow (typically 1 cm/day of flapping amplitude increase) because solar pressure forces are weak. The instability can be avoided all together by choosing a ratio of collector mass over combiner mass different from 3/2.

Damping of Tether Oscillations

One issue for precision formation flying is the tether dynamics and, consequently, the ability to damp out tether oscillations excited by maneuvers. Longitudinal tether waves (i.e., stretch

modes) are negligibly small because of the tether high stiffness and are rapidly damped by the tether material friction. Lateral vibrations, that are typically excited by retargeting maneuvers, can be damped out by vibration dampers located at the attachment points of the tethers to the spacecraft. The damping strategy planned for SPECS utilizes a mass-spring-dashpot system mounted at each tether attachment point to the collector spacecraft (see Fig. 6a). If only internal forces are used for tether oscillation damping, then the total angular momentum of the formation is conserved and the formation pointing direction does not drift from its average value.

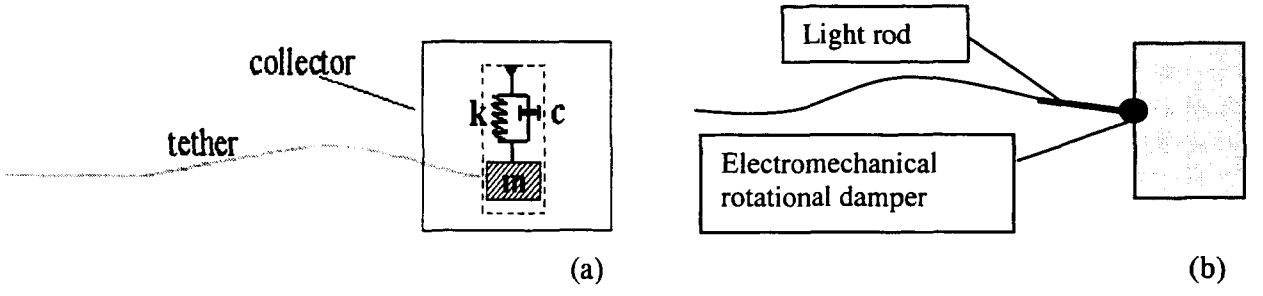

Figure 6 Attachment-point tether damper: (a) physical model, and (b) schematic of possible mechanization.

The transverse-wave damper can be engineered, at a conceptual level, as a light rod of 1-2 m length that is hinged at the spacecraft to rotate about two axes (see Fig. 6b). The tether is held by small pulleys at the tip and the base of the rod (like in a fishing rod) so that the rod follows the side motion of the tether while the tether is free to be reeled in and out. The hinges at the base will be mechanized with electromechanical devices in which the rotational stiffness and damping can be adjusted by changing electrical parameters over a wide range of values.

The transfer of energy carried by the waves from the tether to the passive damper is maximized when the tether wave impedance is matched to the damper impedance (Miller and Hall, 1991). The impedance of transverse tether waves, whose attenuation in the vacuum of space is negligible, is:

$$Z_1 = \mu v \tag{1}$$

where $v = (T/\mu)^{1/2}$ is the wave propagation velocity, T the tether tension, and μ the tether linear density. The impedance of the damper system that is forced to move by the tether at the wave angular frequency ω is:

$$Z_2 = c + i(m\omega - k/\omega) \tag{2}$$

where m, c, and k are the damper's mass, damping coefficient, and spring stiffness, respectively. The matching of the damper's impedance to the transverse wave impedance, $Z_1 = Z_2$, yields:

$$\mu v = c + i(m\omega - k/\omega) \tag{3}$$

which, in turn, implies $m\omega - k/\omega = 0$ and $c = \mu v$. The impedances can be matched by either: (a) m = k = 0 and $c = \mu v$, i.e. a massless, dashpot-only system; or (b) $\omega = \omega_0 = (k/m)^{1/2}$ and $c = \mu v$, provided by a massive damper system with a natural frequency tuned to a specific wave frequency. Condition (b) can be more realistically implemented than condition (a).

Note that the damper's damping coefficient, with matched impedance, does not depend on the wave frequency but it does depend on the wave propagation velocity v, and hence, on the tether tension. In other words, the viscous part of the impedance matching is valid for all waves propagating in a non-dispersive medium, like a continuous string, but the match must be adjusted for different values of tether tension. Note that dampers that require tuning to a broad range of frequencies must be electro-mechanical in order to have an adequate dynamic range.

The classical equations that describe the transmissibility of waves at the transition between two media with different propagation characteristics can be applied to case (b) above (Pain et al. 1983). The wave transmissibility function has the same formulation of the energy loss per damping cycle of waves propagating along a tether terminated with a spring and dashpot massive damper, as computed in Beletsky and Levin (1993).

Figure 7 shows the fractional reduction of the wave amplitude per damping cycle ($\delta A/A$), derived from the wave transmissibility function, for cases of maximum and minimum baseline lengths of the interferometer. Note also that the tangential velocity of the collector spacecraft (with respect to the system center of mass) was assumed equal to 2.15 m/s and 0.04 m/s at the maximum and minimum baselines, respectively, in order to maintain the angular rotation rate of the interferometer approximately constant during an observation, as currently planned.

In either case, the damper is tuned to the first modal frequency of the transverse waves and the first mode is damped in one damping cycle (D_{cycle}), that is, the time that the wave takes to travel back and forth along the tether at the relevant propagation velocity. Higher modes take more than one cycle to damp out but, generally speaking, a damper with light mass (let us say 200 grams) can damp very effectively higher-order modes over a few damping cycles, especially at long baseline lengths.

As the length of the baseline decreases and the wave frequencies increase, the damping of higher modes takes more cycles. However, the duration of a damping cycle is substantially shorter at short baselines so that the overall time for damping is comparable to the long baseline cases.

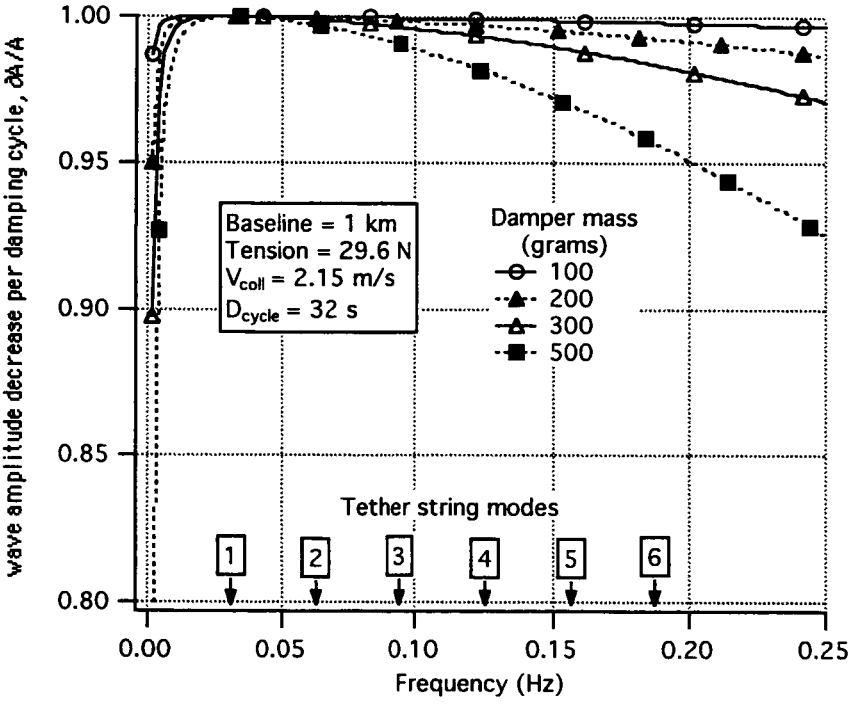

(a)

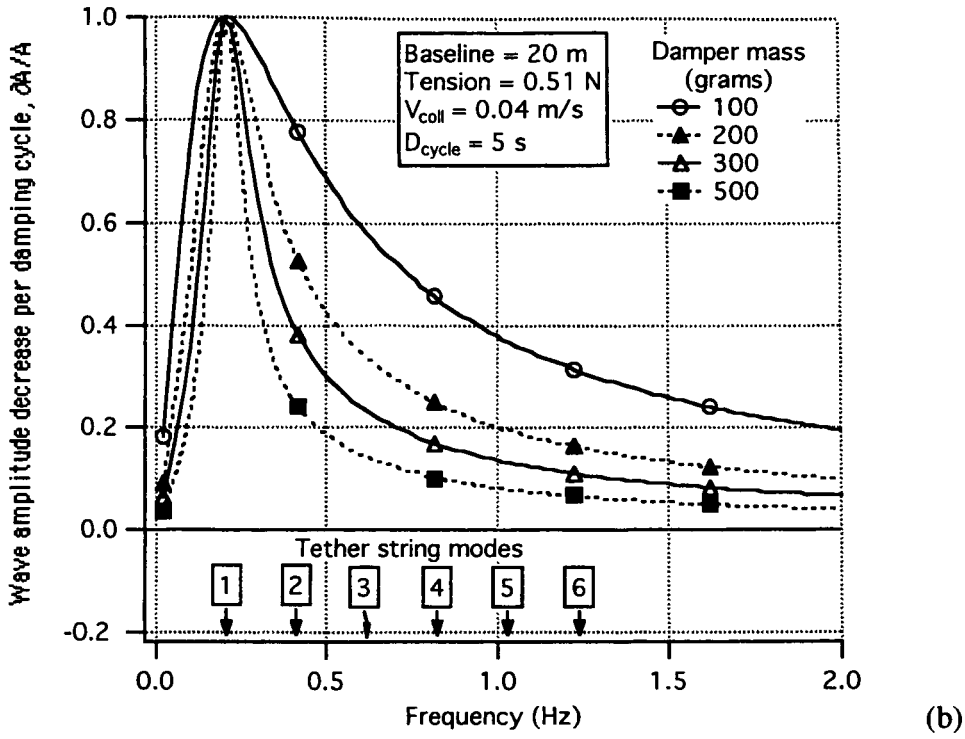

Figure 7 Wave amplitude reduction per damping cycle vs. wave frequency for different masses of the tether attachment point damper at: (a) baseline length = 1 km and collector's tangential velocity = 2.15 m/s; and (b) baseline length = 20 m and collector's tangential velocity = 0.04 m/s.

Numerical Simulations of Tether Oscillations Damping

The analytical results shown previously were confirmed through numerical dynamics simulations (see also Lorenzini, Bombardelli, and Quadrelli; 2001) of the interferometer at a 1-km baseline. Figure 8 shows the transverse oscillation amplitude, measured at the tether mid point starting from large perturbations of the tether transverse oscillations. The impedance-matched damping system rapidly abates the lateral oscillations as expected. Note also that transverse oscillation amplitudes of about 20 cm (as shown in Fig. 8a) are very conservative. Those values can only be obtained with thrusters stuck open on one collector spacecraft, after having assumed a thrust level five folds higher than what is presently considered for retargeting and reconfiguration maneuvers.

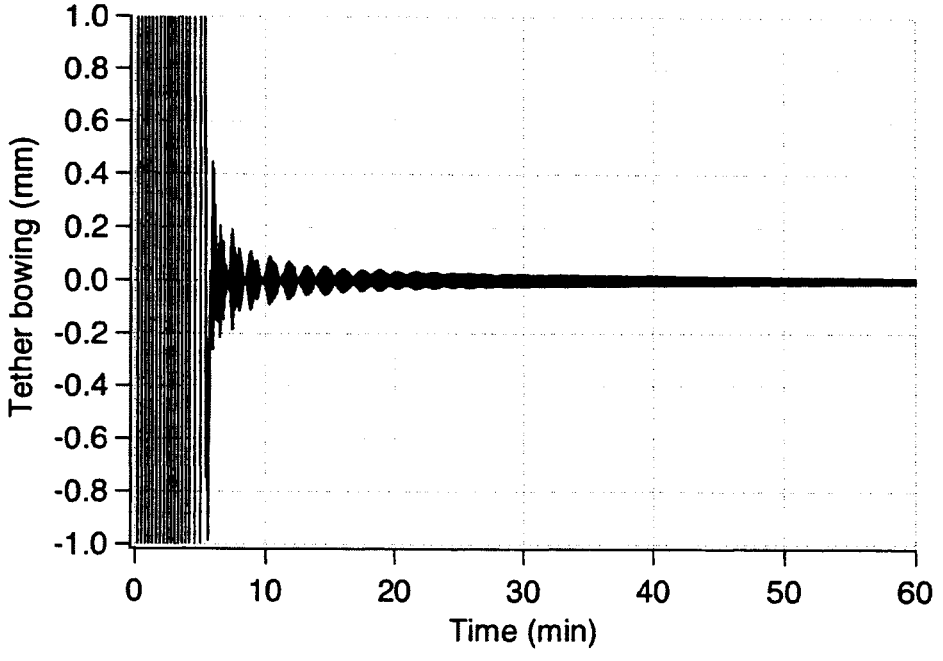

(a)

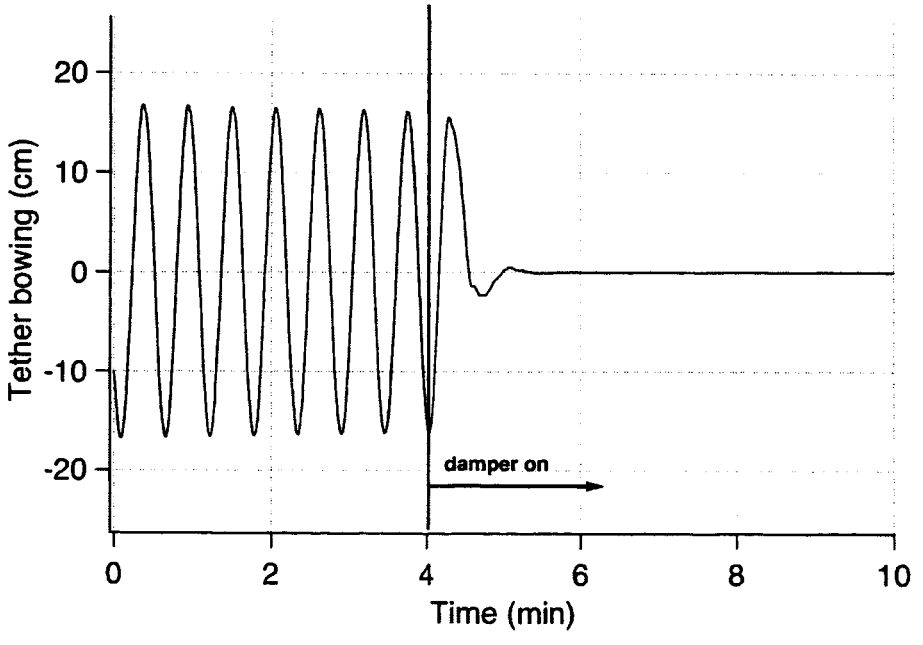

(b)

Figure 8 Damping of tether transverse oscillations (at mid point of a tether branch) according to numerical simulations: (a) long-term response; and (b) zooming around the time of transverse damper activation.

Influence Coefficients

The arrival delays between the wave fronts of the light beams from the collectors are corrected by the delay lines at the combiner to produce interferometric fringes. The delay lines, however, have a stroke length of several centimeters only and, consequently, the tethers have to maintain the formation within that length. More specifically, the differential distance (or equivalently the optical path delay, OPD, in short) between each collector and the combiner has to be maintained within a few centimeters. The various vibrations modes of the tethers have different influence on that differential distance as follows: symmetric (between the left and right tether branches) modes produce a null error; and anti-symmetric modes produce non-null errors. The impact of the modal amplitudes upon the OPD is determined by geometry and it can be simply expressed by influence coefficients. The influence coefficient for an anti-symmetric longitudinal (e.g., along the tether) modes is equal to one. Fortunately, the natural longitudinal modes are small thanks to the stiffness of the tethers and, moreover, they are damped out by internal friction. The forced longitudinal tether oscillations are associated with thermal stretches which are for the most part symmetric. Asymmetries arise from differences in the optical coefficients between the two tether branches which will be small because the two tethers are made of the same material.

The case of tether lateral modes (e.g., string-like) is more interesting. Anti-symmetric lateral modes, for example, are excited by retargeting maneuvers. The oscillations are abated in a few minutes by the lateral vibration dampers. Nevertheless, it is worth noting that the influence coefficients of the lateral anti-symmetric tether modes are very small. Figure 9 shows the ratio between the OPD and the lateral oscillation tether amplitude. It is worth noting that the ratio depends quite linearly on the mass ratio of the tether mass over the collector mass. Since the mass ratio is at most of order 10^{-3}, the influence coefficients of lateral oscillations upon the PD difference are small.

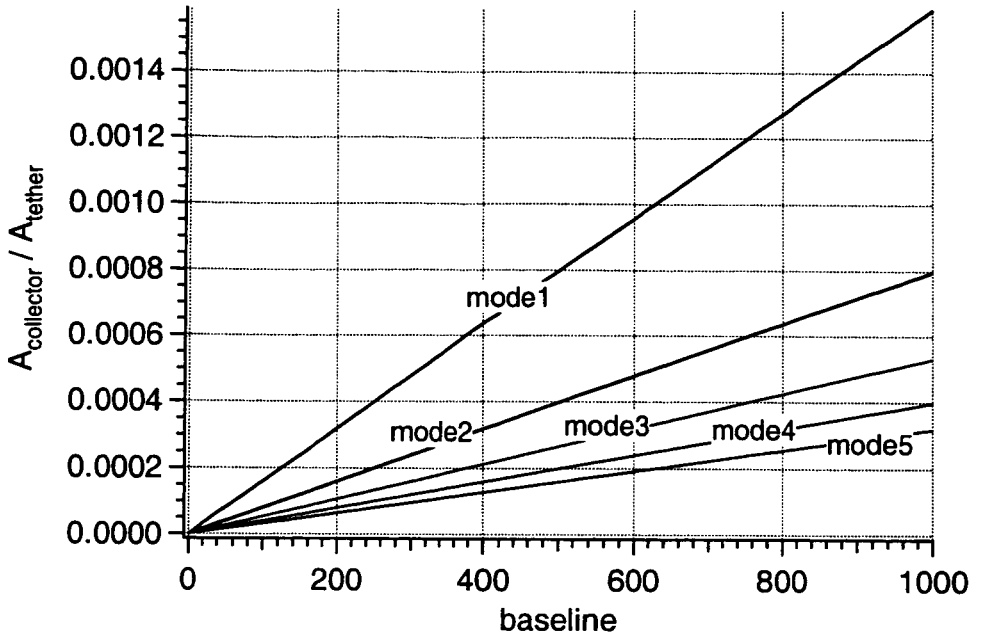

Figure 9 Influence coefficients of lateral tether oscillations, i.e., ratio of collector displacement (directly related to the OPD) over tether lateral oscillation amplitudes for various modes.

In the following, we quantify the values of expected OPD differences arising from a worst-case operational scenario. In this scenario, we assume that a pair of thrusters on board the collectors are firing, in a step-like fashion, in opposite direction, orthogonally to the spin plane. Figure 10 shows the OPD (in millimeters) that results from this step-like actuation of the thruster pair. This actuation scenario is equivalent to an abrupt retargeting maneuver in which the thrust level is not smoothed out according to the desired retargeting control law (see later on).

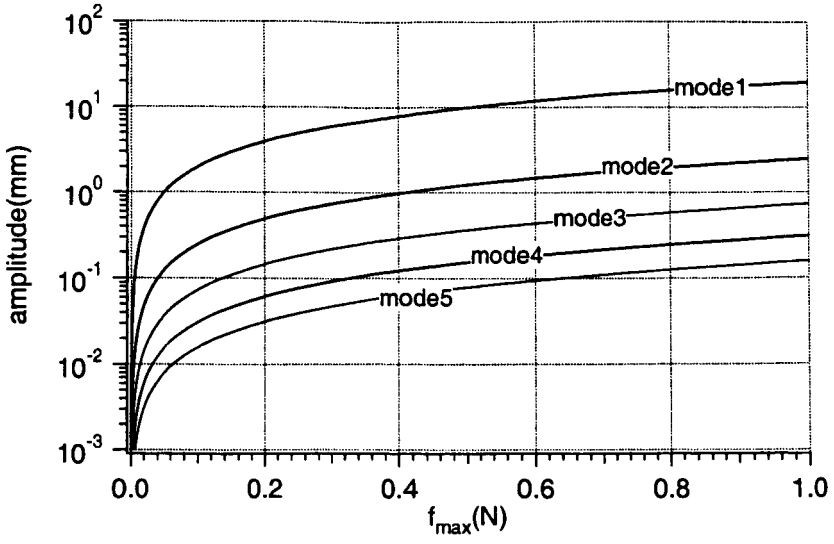

Figure 10 Optical Path Delay resulting from abrupt actuation of a pair of thrusters on board collector thrusting in opposite direction (see text).

Note that in the present design of SPECS the maximum thrust of the retargeting thrusters is 0.2 N and, consequently, in the worst-case retargeting scenario the lateral oscillations (without any damping) would produce an OPD difference of less than 1 cm.

Simulations of Formation Dynamics

Brief description of simulator code

The simulation code that has been used to analyze the SPECS dynamics is the SAO code MASTER which has been utilized for mission development and tested on data of previous tether flights (TSS-1, TSS-1R, SEDS-I, SEDS-II and TiPS). The code has the following characteristics:

- Lumped-mass model of the tether (discretization most widely used in tether simulators)
- Gravity field at L-2
- Third-body gravity perturbations
- Solar radiation pressure
- Tether thermal model with Earth's IR, solar illumination, emitted radiation, thermal capacity of tethers, and *ohmnic heating

*Attitude dynamics of one spacecraft

*Atmospheric density: MSIS '86 model

*Plasma density: IRI '95 model

*Magnetic field: IRGF '85 model

*Orbital Motion Limited (OML) electron collection model for bare electrodynamic tethers

*Parker-Murphy electron collection model for spherical anodic terminations

**Routines not used in the SPECS simulations*

The simulation of SPECS dynamics has been carried out by using 30 lumps to discretize the tether which amounts to 90 tether oscillation modes. Three more lumped masses were used to model the two collectors and one combiner with an overall number of 99 degrees of freedom for the discretized model.

Numerical simulations

The numerical simulation were carried out at 1-km nominal baseline length to show the dynamics induced by temperature variations, gravity gradients, and transverse oscillations. The formation was assumed to be pointed 20° off the anti-solar direction in order to maximize environmental perturbations. The temperature fluctuations (Fig. 11a) of the tether dominate the baseline variations (Fig. 11b) with negligible contributions from gravity gradients and transverse tether dynamics. Note that the effect of tether bowing on the baseline length, and ultimately on the optical path delays, is strongly attenuated by the tether/spacecraft mass ratio as shown previously. Note also that the Spectra-2000 material, considered here as a potential tether material candidate, has a negative thermal expansion coefficient.

The long stroke of the delay line in the optical system allows for the equalization of path length difference between the two arms of the interferometer, and a separate mechanism provides fast (>1 Hz) path length difference corrections. The ranges provided by these mechanisms are much greater than the predicted tether-induced variations.

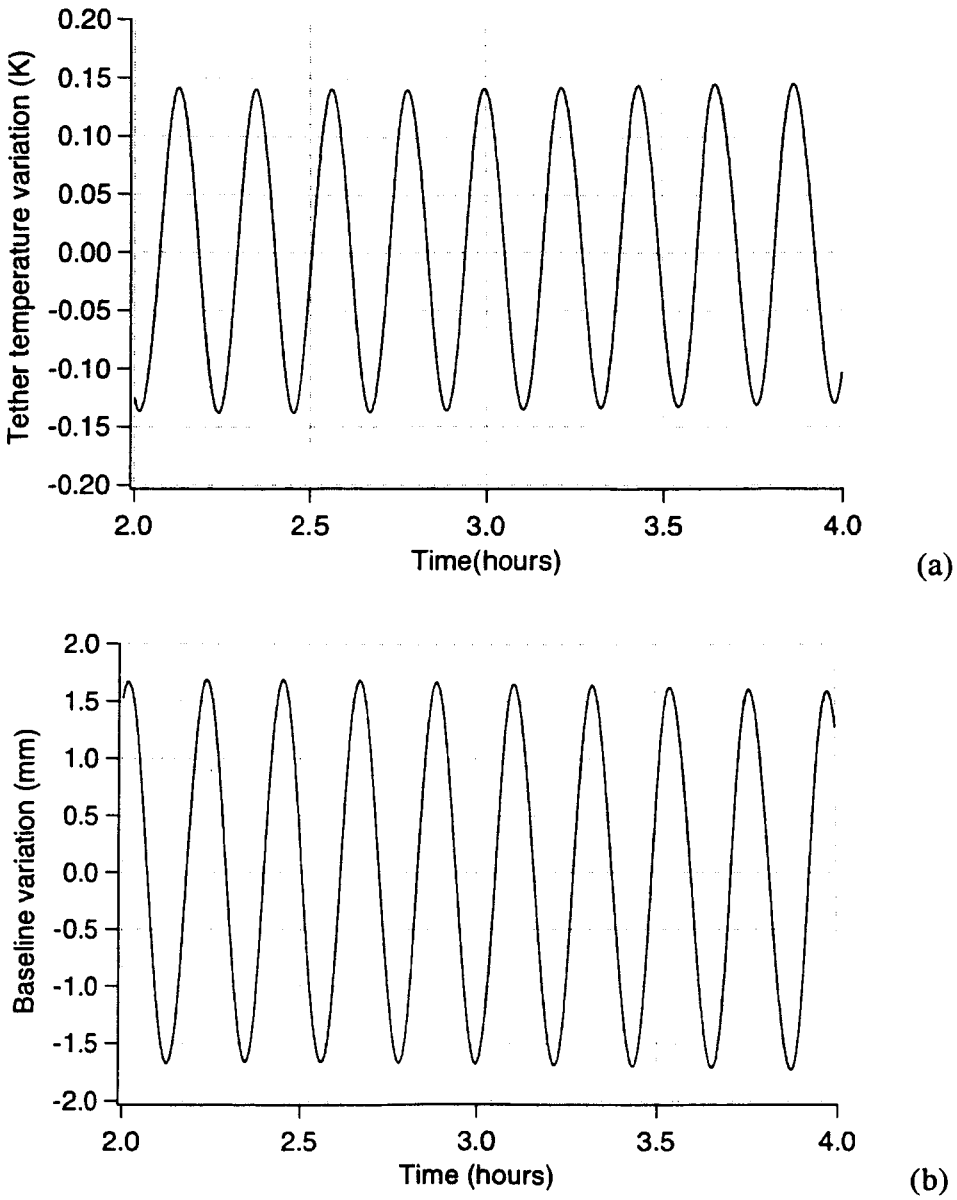

Figure 11 Steady-state response of the tethered formation at L2 during a SPECS observation at 1-km baseline length: (a) tether temperature fluctuation; and (b) variation of baseline length (from collector to collector).

Strategy for Fast Formation Retargeting

Fast retargeting maneuvers

Retargeting of the interferometer can be accomplished by precessing the angular momentum vector of the formation. Thrusters are activated on the collectors near the desired nodal line of the formation plane's rotation. The thrusters produce a torque at 90° to the nodal line so that the angular momentum vector rotates about the nodal line (Fig. 12).

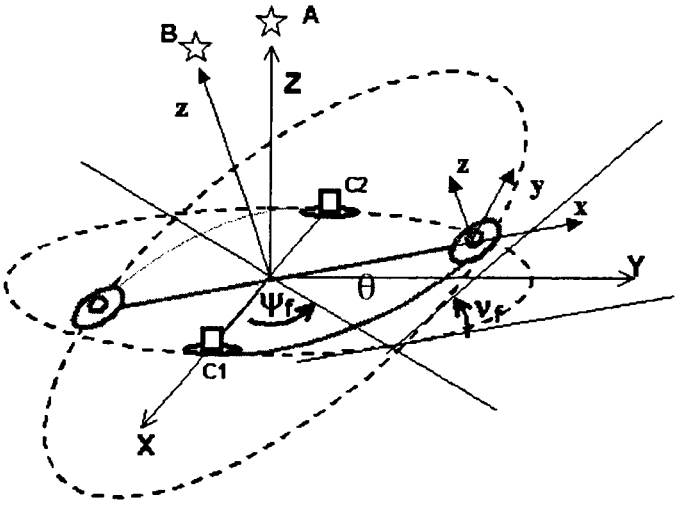

Figure 12 Schematic of retargeting maneuver by precessing the formation's angular momentum

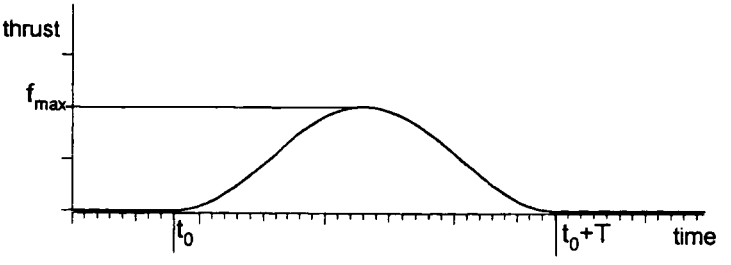

Figure 13 Thruster actuation profile

In a previous work (Ref. [i]) we derived control laws for steering accurately the interferometer from one target to another separated by an angle of several degrees. Here we apply that control

strategy to a retargeting of SPECS with a 5° separation between the two targets. Figure 13 shows the thruster actuation profile about the nodal line.

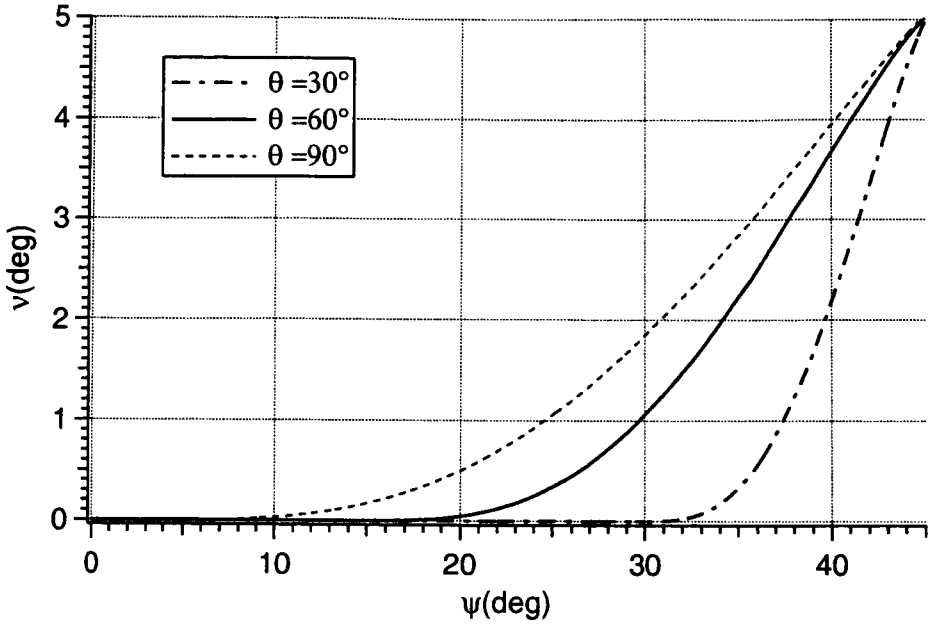

Figure 14 Time histories of nutation vs. precession angle for a thruster actuation arc length ranging from 30° to 90°.

The thruster force law is as follows:

$$F_{thr} = f_{\max} \sin^2\left[(t - t_0)\pi / \Delta T\right] \tag{4}$$

where $\Delta T = \theta/\omega$ is the thruster actuation time, θ is the thruster actuation arc length, ω the spin rate of the interferometer, and f_{max} the maximum thrust force given by:

$$f_{\max} = 2m\omega^2 R \cdot \Delta v / \theta \tag{5}$$

where m is the collector mass, ω the spin rate, R the collector's radius of rotation and Δv the retargeting angle.

For the present collector mass of 3200 kg and a thruster actuation arc length ranging from 30° to 90°, the maximum thrust force ranges from 8.5 N to 2.8 N at a baseline length of 1 km (i.e., R = 500 m) and from 0.17 N to 0.06 N at a baseline length of 20 m (i.e., R = 10 m). With a

spin period of 26 minutes (as presently envisioned for SPECS), the retargeting maneuver that follows the strategy previously outlined can be accomplished in a time ranging from 2.2 to 6.6 minutes. As electrical thrusters are planned to be utilized for the attitude and formation control of SPECS, the technique for fast retargeting maneuvers will exceed the thrust level (now at 0.2 N) at long baseline lengths. However, the technique could be used profitably for baseline lengths of less than 80 m, after having assumed a thruster actuation arc length of 90° and a maximum retargeting angle of 5°. For baseline lengths longer than 80 m, the periodic-thrusting technique developed by Farley (see Ref. [ii]) should be used. That technique utilizes low-thrust levels modulated over several full rotations of the interferometer.

Retargeting maneuvers will excite the tether lateral oscillations. However, since the tether is comparatively light and the tether tension relatively strong (especially at long baseline lengths), the amplitude of the final tether lateral oscillations are relatively modest as shown by numerical simulations (Fig. 15). Those oscillations will be quickly damped by the tether attachment point dampers.

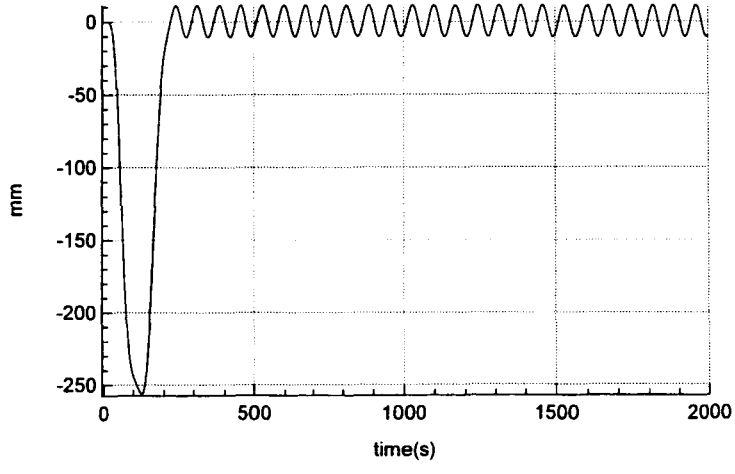

Figure 15 Amplitude of lateral oscillation at the mid point of a tether branch after a retargeting maneuver.

Furthermore, retargeting maneuvers can be optimized in terms of duration time span so that the final lateral oscillations of the tether branches are minimized (the maneuver shown in Fig. 15 is not optimized). The optimal strategy can be viewed as an impulse shaping technique in which a time-portion of the thruster actuation produce positive work on the tether oscillation and the

remaining portion an equivalent amount of negative work to cancel out the oscillation of several lateral modes. The optimized retargeting strategy is discussed in Ref. [iii].

Propellant consumption for retargeting maneuvers

The thrusters location on the collector spacecraft can produce a high torque with relatively small thrust forces and, consequently, relatively small propellant consumption. From the precession of the angular momentum vector and the rocket equation we obtain the fuel consumption per collector throughout the mission:

$$m_{fuel} = m \cdot \left[\exp\left(\frac{\omega RN \cdot \Delta v_{ave}}{\eta g I_{sp}} \right) - 1 \right] \tag{6}$$

where N is the total number of targets, Δv_{ave} the average retargeting angle, η the efficiency of the retargeting maneuver (which is greater than 0.95), and I_{sp} the thruster's specific impulse.

We assume ω = constant = 0.004 rad/s, N = 1500 (targets), η = 0.95, g = 9.8 m/s^2, I_{sp} = 2500 s (for ion thrusters) and $\Delta v_{ave} = 5°$. Moreover, we assume that half of the retargeting maneuvers are done at the minimum radius of 10 m and the other half at the maximum radius of 500 m. Finally, we obtain that the propellant necessary for carrying out 1500 retargeting maneuvers is about 0.6% of each collector mass. The propellant required for retargeting at the minimum radius (or baseline length) is very small and, consequently, most of the (modest) propellant consumption is for the retargeting maneuvers carried out at the maximum baseline length.

Tether Survivability to Micrometeoroids

Micrometeoroids model

In a heliocentric orbit far away from Earth there are micrometeoroids and no man-made orbital debris. Since $R >> R_E$ (where R is the distance from Earth and R_E the equatorial radius), the gravitational focusing of micrometeoroids and the shielding provided by Earth are negligible. In this case, the interplanetary micrometeoroid model can be applied directly without any correction factors. The model adopted for the micrometeoroid flux is the Grun[iv] interplanetary model (see Figure 16) The flux shown in the figure is the cumulative flux, that is, the flux of particles with diameter equal or greater than the diameter indicated on the abscissa.

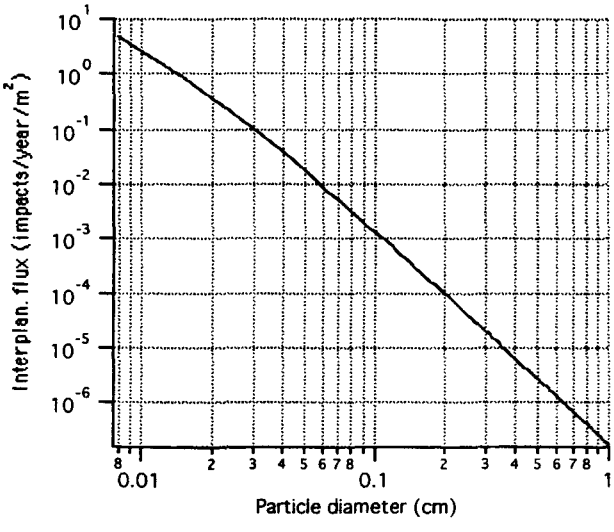

Figure 15 Integrated flux of micrometeoroids in interplanetary space.

After assuming a Poisson distribution of events, the expression of the survival probability for a single-line tether is:

$$\chi = 1 - e^{-\alpha} \tag{7}$$

where $\alpha = FAt$ is the critical-impactor impact rate for the single tether, in which F is the critical-impactor flux (as explained later on), A is the wet surface of the tether (because micrometeoroids have a fairly isotropic distribution) and t is the exposure time. The critical impactor diameter for cylindrical tethers is assumed (from hypervelocity experiments) to be equal to 1/3 of the tether diameter and, consequently, Figure 1 can be used to compute the critical impactor flux F.

Error! Reference source not found.17 shows the survival probability for a single-line (yet multi-filament) 1-km-long tether vs. the tether diameter for different values of mission duration. Figure 17 clearly shows that a single-line tether will have a relatively low survival probability

over several years unless the single line is rather thick. For example, a line diameter of about 6 mm would be needed for a 1-km tether to survive in space for 5 years with a probability of about 99%.

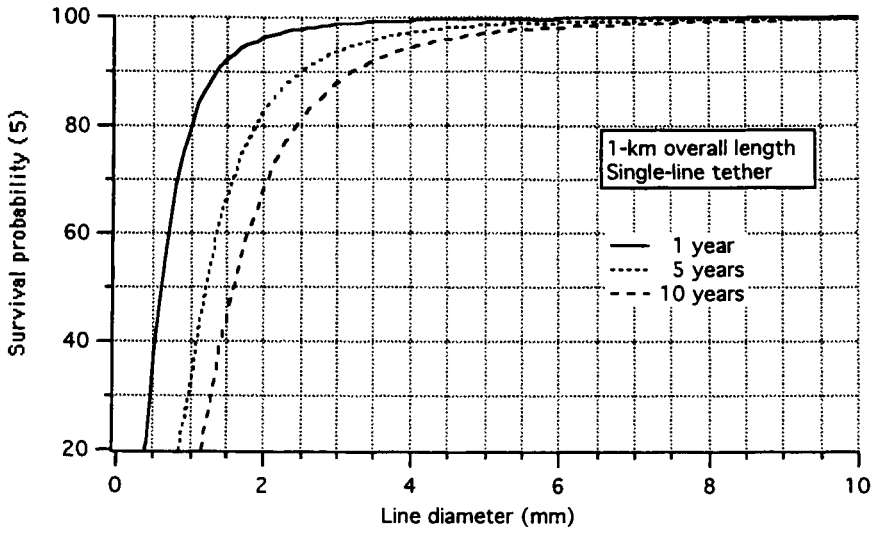

Figure 16 Probability of survival of single-line, 1-km-long tether vs. tether diameter for different values of mission duration.

Survivability using multi-line tethers

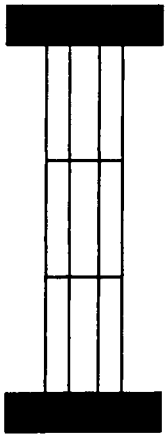

Figure 16 Schematic of multi-line, fail-safe tether with $m = 3$ cells and $n = 4$ lines.

A way to increase the tether probability of survival to micrometeoroid impacts without using massive tethers is by using a multi-line (i.e., redundant) tether configuration. The multi-line tether configuration can be seen, from a modeling point of view, as a grid. A grid tether consists of a set of n (vertical) lines connected to each other at (m + 1) points so that the tether structure is composed of m cells and n lines as shown in Figure 18. The n lines have the same diameter d and approximately the same length L.

If we consider a grid tether of n lines and m cells, the probability of failure of one line in one cell is given by the following formula after considering that the exposed area of a single tether segment is A/m.

$$\chi = 1 - e^{-\frac{\alpha}{m}} \tag{8}$$

The combined failure probability of the n segments forming a cell is

$$\chi = \left(1 - e^{-\frac{\alpha}{m}}\right)^n \tag{9}$$

Consequently, the survival probability of a single cell is simply:

$$P = 1 - \left(1 - e^{-\frac{\alpha}{m}}\right)^n \tag{10}$$

Since the tether consist of m cells, the combined probability of survival of the whole tether is

$$P_{mn} = \left[1 - \left(1 - e^{-\frac{\alpha}{m}}\right)^n\right]^m \tag{11}$$

Tether Conceptual Design

Survivability to Micrometeoroid Impacts of Various Tether Designs

A number of configurations suitable for SPECS have been analyzed to evaluate the probability of survival to micrometeoroids in interplanetary space (i.e., at L-2). The tether system for the present SPECS architecture consists of two branches of 500-m max length and, consequently, we will assume an overall tether length of 1 km. The three configurations are:

a) single-line tether;
b) 2-parallel-line tether with lines interconnected every 100 m;
c) 4-parallel-line tether without interconnections within a branch.

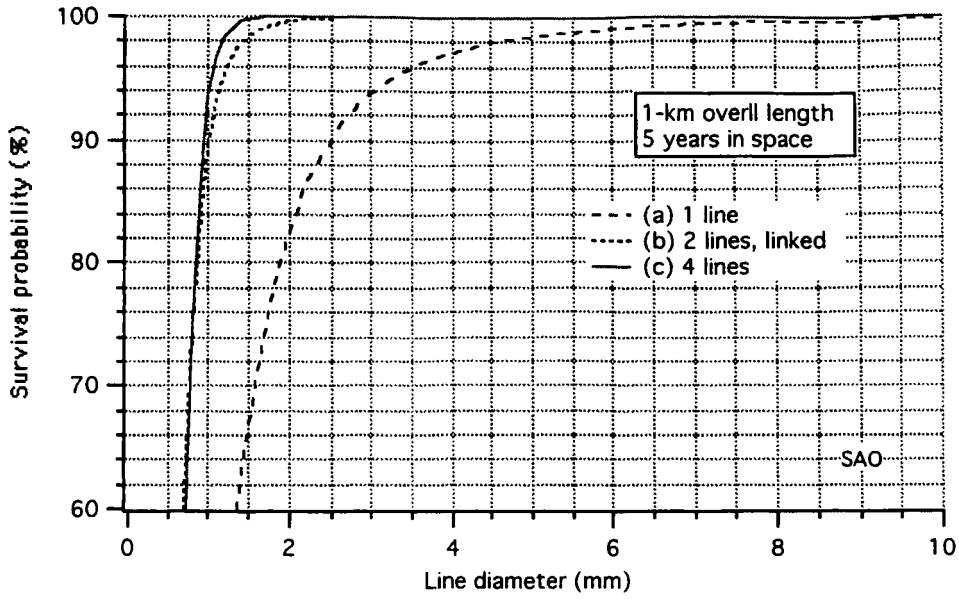

Figure 17 Probability of survival for tether configurations (a), (b) and (c) (see text).

Figure 19 shows the probability of survival of the three tether designs vs. the diameter of each tether line, exposed in space for 5 years As expected a multi-line tether configuration has a much better probability of survival than a single-line configuration if we assume same diameters for the single-line and the multi-line tether (which is actually unfair for the single-line tether). When we compare the configurations based on equal tether mass (see Fig. 20), the results are less skewed towards the multi-line configurations but still favor strongly the latter configurations with respect to the single-line tether.

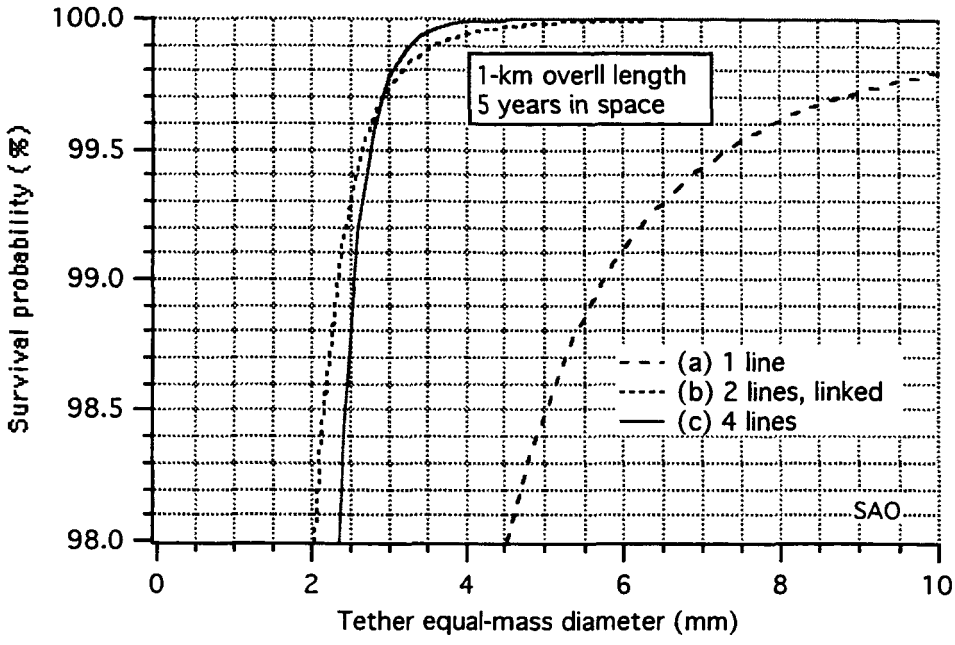

Figure 18 Survival probability to micrometeoroids impacts based on equal tether mass

For example, a 4-line, 1-km tether (without cross linkages) with each line diameter equal to 1.5 mm (i.e., an equal-mass diameter of 3 mm) could survive the micrometeoroid interplanetary flux over 5 years with a probability close to 99.8%. A 2-line, 1-km tether with cross linkages every 100 m and line diameters of 2.12 mm (that is, same mass of the previous one) could survive the micrometeoroid flux with a probability of about 99.7%. In other words the micrometeoroid survival issue can be solved by adopting a multi-line tether design, and the lines do not need to be interconnected, within a tether branch, for the tether lengths of interest to SPECS.

Tether Mechanical Strength

The mechanical strength of multi-filament (where a filament should not be confused with a tether line which is made of many filaments) ropes is measured in grams/denier (GPD) or centiNewton/decitex (cN/Tex) where the denier is the weight in grams of a 9,000-m rope and the decitex is the weight in grams of a 10,000-m rope. These are units used by the textile industry and, although a little strange at first sight, they are justified by the fact that the outside diameter

(which would be typically used to express the strength of a solid bar) is neither well defined nor measurable in deformable, multi-filament ropes.

Table 1 Characteristics of some suitable tether materials[v]

Material	GPD at yield (grams/denier*)	Density, ρ (kg/m^3)	Tensile strength, σ (GPa)	Characteristic length[¥] (km)	Characteristic velocity[§] (m/s)
PBO (Zylon)	42	1560	5.8	380	2730
Spectra 2000 Dyneema SK75	40	970	3.4	350	2660
Spectra 1000 Dyneema SK60	35	970	3.0	315	2490
Kevlar-29 & 49	22	1440	2.76	195	1960
Steel	3	7800	2.1	27	730

*Denier is weight in grams of a 9000-m long rope
¥Length at yield of tether in 1-g field = $\sigma/(\rho g)$
§Tip velocity of a rotating tether at yield = $\sqrt{2\sigma/\rho}$

A parameter that defines the mechanical quality of a material for aerospace application is the yield strength over density ratio. The ratio has the units of $(m/s)^2$. An alternative way of expressing the same quality factor is the tip velocity of a rotating tether at which a cylindrical tether will reach its yield strength at the hub. This quantity is often called the characteristic velocity of the material. Another way of expressing the same quality factor is the characteristic length of the material which is the length at yield of a constant-cross-section cable suspended vertically in a uniform 1-g field. Table 1 shows the values of key parameters of materials suitable for space tethers, where we have included Steel for matter of comparison.

The GPD allows to compute readily the weight of a tether/rope with a desired breaking strength (expressed in kilograms force). We also have to consider that the GPD shown in the table is for a constituent element of a rope (also called a tow) that is a small bundle of filaments twisted together, typically with a denier of 100-200. The GPD of an actual rope, which is made of many tows, can be conservatively assumed to be somewhat lower than the single tow GPD (we will assume 90% of the tow strength in the following computations). As an example, a 1-km-long rope made of Spectra 2000 (or alternatively Dyneema SK75) with a breaking strength (at room temperature) of roughly 3.7 metric ton, would weigh about 10 kg. We should also keep

in mind that the strength of Spectra material increases with decreasing temperature. In space applications, Spectra and Dyneema run very cold because of their low absortivity/emissivity (α/ε) ratio and, consequently, the breaking strength in space will be higher than what was shown in the above computation.

Tether Design Concept

It is premature to speak about a tether design because the design is indeed affected by many considerations that can not be evaluated at this point like wear and tear and degradation in space. However, we will show in the following a possible tether concept for SPECS (see Figure 21).

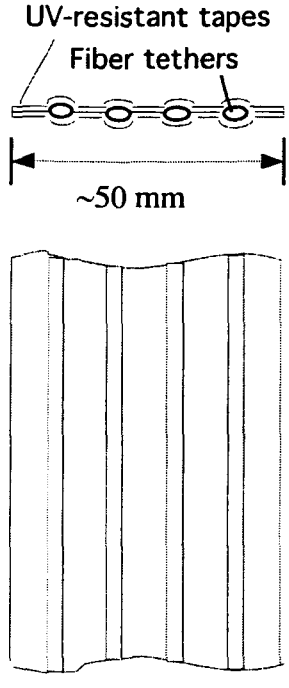

Fig. 18 Cross section and plan view of possible SPECS tether tape configuration

The conceptual tether system consists of 4 tethers, each with an oblate (or better flattened) cross section. The tethers run parallel to one another and are sandwiched in between two thin layers of (almost transparent) tapes made of UV-resistant material. The result is a relatively light and strong ribbon tether system that will have an excellent probability of survival to micrometeoroid impacts. A ribbon geometry was indeed used by the Naval Research Laboratory (NRL) for the tethered spacecraft ATEx in 1999. The ribbon tether of ATEx used 3 thin (~0.2-mm-diameter or 215 denier) tethers sandwiched between two thin polyethylene strips to form a 'ribbon tether' with a width of 1 inch. The tether for SPECS will use thicker tethers, each with a denier of 30,400 (i.e., an equivalent-cylinder diameter of roughly 2.5 mm) and a tape wider than the ATEx ribbon. A preliminary analysis of such tether system estimates a breaking strength, at beginning of life, in excess of 4.86 metric ton and a probability of survival to micrometeoroid impacts well above 99.9%. The mass of the fibers is presently estimated at 13.5 kg with another 7 kg allocated for the tape material, plus the mass of adhesive (if needed). In conclusion, we can estimate the total mass of the 1-km-long ribbon tether to be less than 30 kg.

If we assume a SPECS collector mass of 3200 kg, a maximum tangential velocity of 2.15 m/s at 500-m radius, then the maximum steady tether tension is about 30 N or equivalently about 3 kg force. Consequently, the mechanical safety margin of the whole tether is very large with respect to the *steady maximum tension* expected during observations. Even if three of the tether/ribbon lines fail, the remaining single line will have a mechanical safety margin much greater than the load margin of 5 specified by NASA for unmanned tethered missions[vi].

Several other considerations come into play when designing a tether system that has to last several years in space and undergo many mechanical cycles of spooling and unspooling. Some of the issues will require ground experimentation in a representative test bed in order to estimate the wearing and tearing and to help in selecting the right material and bonding process for the tapes.

The conceptual design described here indicates that it is possible to conceive a tether system with a breaking strength, at the beginning of life, that exceeds the maximum load of SPECS by a very large margin, an excellent probability of survival to micrometeoroid impacts, and a comparatively light mass.

Conclusions

The results of our dynamics analysis of SPECS are very encouraging. The tethered linear configuration in orbit at L2 is very stable. The tethers can maintain the distances between the two collectors, during steady rotation of the interferometer and for realistic environmental conditions, to within 1 cm, and the optical path delays to an even smaller value. We have developed a conceptual design of light-mass oscillation dampers for damping out the transverse tether oscillations which result from retargeting maneuvers and off-nominal behavior of retargeting thrusters. The analysis of the dynamic response of the tethers attached to the dampers demonstrated that comparatively large tether transverse oscillations (excited by off-nominal operations) can be damped out in a few minutes.

We have also developed control laws for the fast retargeting of the interferometers at moderate baseline lengths, and our colleagues at NASA GSFC have developed (slower) techniques that are more suitable for the longer baseline lengths. We have also computed the propellant necessary for retargeting the tethered interferometer to 1500 targets during its lifetime to find out that the propellant required is less than 1% (over the lifetime) of each collector spacecraft.

Finally, we developed a conceptual design of a high-strength tether, with a multi-line, redundant geometry capable of surviving micrometeoroid impacts at L2 over a 5-year lifetime with an estimated probability of survival better than 99.9%.

References

[i] Harwit, M. (PI) et al., "Kilometer-Baseline Far-Infrared/Submillimiter Interferometer Vision Mission." Final Report to NASA, May 2005.

[ii] Bombardelli C., E.C. Lorenzini and B.M. Quadrelli, "Retargeting Dynamics of a Linear Tethered Interferometer." Journal of Guidance, Control and Dynamics, Vol. 27, No. 6, 1061-1067, 2004.

[iii] Farley, R., "Study for the in-plane thrust and fuel requirements of a 2-collector system using electric propulsion with constant thrust." Presentation, January 2005

[iv] Lorenzini, E.C., C. Bombardelli and M. Quadrelli, "Analysis and Damping of Lateral Vibrations in a Linear Tethered Interferometer." Advances in the Astronautical Sciences, Vol. 114, pp. 1627-1636, *Spaceflight Mechanics 2003*, AAS Publications by Univelt, San Diego, CA, 2003.

[v] Grun, E., Zook, H.A., Fectig, H., Giese, R.H., "Collisional Balance of the Meteoritic Complex." Icarus, Vol. 62, pp. 244-272, 1985.

[vi] Data collected from several material data sheets including data from DuPont, Toyobo, Honeywell, Cortland Cables, and Materials Engineering: *Materials Selector* (Penton Publication, 1993).

[vii] Tomlin D.D., G.C. Faile, K.B. Hayashida, C.L. Frost, C.Y. Wagner, M.L. Michell, J.A. Vaughn, and M.J. Galuska, "Space Tethers: Design Criteria." NASA TM 108573, July 1997.